2MTF - VII. 2MASS Tully-Fisher survey final data release: distances for 2,062 nearby spiral galaxies

Tao Hong [1,2,3,4⋆], Lister Staveley-Smith [3,4,5], Karen L. Masters [6], Christopher M. Springob [3,4,7], Lucas M. Macri [8], Bärbel S. Koribalski [9], D. Heath Jones [10], Tom H. Jarrett [11], Aidan C. Crook [12], Cullan Howlett [3,4] and Fei Qin [3,4]

[1]*National Astronomical Observatories, Chinese Academy of Sciences, 20A Datun Road, Chaoyang District, Beijing 100012, China*
[2]*CAS Key Laboratory of FAST, National Astronomical Observatories, Chinese Academy of Sciences*
[3]*International Centre for Radio Astronomy Research, M468, University of Western Australia, Crawley, 35 Stirling Highway, WA 6009, Australia*
[4]*ARC Centre of Excellence for All-sky Astrophysics (CAASTRO)*
[5]*ARC Centre of Excellence for All Sky Astrophysics in 3 Dimensions (ASTRO 3D)*
[6]*Haverford College, Department of Physics and Astronomy, 370 Lancaster Avenue, Haverford, Pennsylvania 19041, USA*
[7]*Australian Astronomical Observatory, PO Box 915, North Ryde, NSW 1670 Australia*
[8]*George P. and Cynthia Woods Mitchell Institute for Fundamental Physics and Astronomy, Department of Physics and Astronomy, Texas A&M University, 4242 TAMU, College Station, TX 77843, USA*
[9]*CSIRO Astronomy & Space Science, Australia Telescope National Facility, PO Box 76, Epping, NSW 1710, Australia*
[10]*English Language and Foundation Studies Centre, University of Newcastle, Callaghan NSW 2308, Australia*
[11]*Astronomy Department, University of Cape Town, Private Bag X3. Rondebosch 7701, Republic of South Africa*
[12]*Microsoft Corporation, 1 Microsoft Way, Redmond, WA 98052, USA*

Accepted ... Received ...

ABSTRACT

We present the final distance measurements for the 2MASS Tully-Fisher (2MTF) survey. The final 2MTF catalogue contains 2,062 nearby spiral galaxies in the CMB frame velocity range of 600 km s^{-1}< cz < 10,000 km s^{-1} with a mean velocity of 4,805 km s^{-1}. The main update in this release is the replacement of some archival HI data with newer ALFALFA data. Using the 2MTF template relation, we calculate the distances and peculiar velocities of all 2MTF galaxies. The mean uncertainties of the linear distance measurements are around 22% in all three infrared bands. 2MTF measurements agree well with the distances from the Cosmicflows-3 compilation, which contains 1,117 common galaxies, including 28 with SNIa distance measurements. Using distances estimated from the '3-bands combined' 2MTF sample and a χ^2 minimization method, we find best-fit bulk flow amplitudes of 308 ± 26 km s^{-1}, 318 ± 29 km s^{-1}, and 286 ± 25 km s^{-1}at depths of $R_I = 20$, 30 and 40 h^{-1}Mpc, respectively, which is consistent with the ΛCDM model and with previous 2MTF results with different estimation techniques and a preliminary catalogue.

Key words: galaxies: distances and redshifts — galaxies: spiral — radio emission lines — catalogs — surveys

1 INTRODUCTION

The matter distribution in the Universe appears to be homogeneous and isotropic on large scales (a.k.a. the cosmological principle). However, on relatively small scales, structures such as clusters, filaments, walls and voids dominate the matter distribution (Geller & Huchra 1989; Gott et al. 2005). Studies of cosmological structures or lack thereof provide tight constraints on the cosmological model (Bernardeau et al. 2002; Jones et al. 2009; Scrimgeour et al. 2012; Lombriser et al. 2012; Alpaslan et al. 2014). Useful information on the matter distribution field can be obtained from galaxy redshift surveys, gravitational lensing studies and X-ray and Sunyaev-Zel'dovich cluster searches (e.g. Eisenstein et al. 2005; Hong, Han & Wen 2016; Bautista et al. 2017; Van Waerbeke et al. 2013; Planck Collaboration et al. 2014a; Salvati, Douspis & Aghanim 2018, and references therein). The peculiar motions of galaxies induced by inhomogeneous matter distribution are also useful probes for tracing structures. These are typically measured using redshift-independent distances (Springob et al. 2007; Masters, Springob & Huchra 2008; Campbell et al. 2014; Tully, Courtois & Sorce 2016), proper mo-

⋆ E-mail: hongtao@nao.cas.cn

tions (Brunthaler et al. 2005) or the kinetic Sunyaez-Zel'dovich effect (Kashlinsky, Atrio-Barandela & Ebeling 2011). Moreover, such measurements trace both the visible and the dark matter distributions (Hong et al. 2014; Scrimgeour et al. 2016; Springob et al. 2016; Qin et al. 2018).

The line-of-sight peculiar velocity is the non-Hubble component of a galaxy's motion, which can be estimated in the nearby Universe by

$$v_{pec} = cz - H_0 r, \quad (1)$$

where H_0 is the Hubble constant, z is the redshift of the galaxy and r is the redshift independent distance. In the context of this paper the Tully-Fisher (TF) relation (Tully & Fisher 1977), which combines measurements of galaxy luminosity and rotational velocity, provides a good tool to accurately measure redshift independent distances for large numbers of spiral galaxies. However, many other distance-determination techniques exist, including supernova type Ia (Phillips 1993), Fundamental Plane (Dressler et al. 1987) and surface brightness fluctuations (Tonry & Schneider 1988).

The SFI++ catalog (Springob et al. 2007) is the largest TF sample to date, and includes peculiar velocity information for 4,861 spirals. Because of the effect of extinction in its input catalogues, SFI++ contains a large gap close to the Galactic plane ($|b| < 15^\circ$). It therefore misses significant parts of massive nearby structures such as the Hydra-Centaurus, Norma and Vela superclusters and the Great Attractor (Kraan-Korteweg & Lahav 2000; Kraan-Korteweg et al. 2017), whilst introducing possible biases in cosmological parameters derived from peculiar velocity fields measured in a non-spherical region (Andersen, Davis & Howlett 2016).

The 2MASS Tully-Fisher Survey (2MTF, Masters, Springob & Huchra 2008; Hong et al. 2013; Masters et al. 2014) uses the infrared magnitudes in the J, H and K bands from the 2MASS Redshift survey (2MRS, Huchra et al. 2012) in order to reduce the extinction effect due to the Galactic plane, leaving only a small Zone of Avoidance at Galactic latitudes of $|b| \leqslant 5^\circ$. Combined with high-quality 21-cm HI spectral data, the final 2MTF sample provides 2,062 peculiar velocity measurements for nearby spirals. In this paper, we present the final 2MTF sample and describe the 2MTF data collection and reduction process in Section 2. The final catalog is presented in Section 3. Comparisons between 2MTF distances and Cosmicflows-3 measurements are made in Section 4. Finally, we update our previous calculations of the bulk flow amplitude for the 2MTF sample in Section 5.

2 OBSERVATIONAL DATA AND METHODOLOGY

The 2MTF survey is a Tully-Fisher survey of nearby spiral galaxies, producing high-quality redshift independent distance and peculiar velocity measurements. The observational methods and data reduction are described in detail by Hong et al. (2014), which we briefly summarise below.

2.1 Photometric data

All target galaxies in 2MTF are selected from the 2MRS catalog with the following criteria: total K-band magnitude $K < 11.25$ mag, velocity $cz < 10,000$ km s^{-1}, and 2MASS co-added axis ratio $b/a < 0.5$. About 6,600 2MRS galaxies meet the selection criteria and became our 2MTF target galaxies. Because the TF template relations vary with the type of spiral galaxy (Masters, Springob & Huchra 2008), we also adopt the morphological type code T to calibrate the galaxies to the correct template relations. The co-added axis ratio used above formally differs from the I-band axis ratio used by Masters, Springob & Huchra (2008) when building the TF template relation. This may introduce small differences in the final measurements, but with no significant bias (Hong et al. 2014). We follow Masters, Springob & Huchra (2008) in making galaxy internal dust extinction and k-corrections.

2.2 HI spectra widths

High-quality galaxy rotation widths as measured from HI spectra are a key part of accurate TF measurements. The 2MTF HI spectral data derive from our own new observations using the GBT and Parkes telescopes, new observations provided by the ALFALFA survey, and high signal-to-noise ratio archival data.

2.2.1 GBT and Parkes observations

The 2MTF project observed 1,193 target galaxies in the sky area of $\delta > -40^\circ$ using the Green Bank Telescope using a position-switching mode (Masters et al. 2014). 727 galaxies were detected in HI, and 383 of them are of a quality that allows them to be included into the final 2MTF catalogue. All the 'well-detected' galaxies have signal-to-noise ratio S/N $\geqslant 10$, and show normal HI profiles consistent with non-interacting, non-confused spiral galaxies. In addition, all galaxies meet further data quality selection criteria as described in Section 2.2.4. The smoothed GBT velocity resolution is 5.15 km s^{-1}.

For $\delta \leqslant -40^\circ$, the Parkes radio telescope was employed to conduct HI observations, also in position-switching mode, but one in which the target galaxy was always observed by one of seven central beams of the Parkes multibeam receiver (Hong et al. 2014). From the 305 target galaxies, we obtained 110 high signal-to-noise ratio HI spectra which were included into the final 2MTF sample. The Parkes HI spectra provide a velocity resolution of 3.3 km s^{-1} after Hanning smoothing.

All HI spectra obtained by GBT and Parkes telescope were measured using the IDL routine *awv_fit.pro*. This routine measures HI line widths using several methods. The W_{F50} width is adopted as our preferred width for this study.

2.2.2 ALFALFA data

Duplication of observations in the northern hemisphere was avoided by leaving the 7000 deg^2 covered in the ALFALFA survey (Giovanelli et al. 2005). Overall, ALFALFA contains $\sim 31,500$ extragalactic HI sources with redshift out to $z < 0.06$ (Haynes et al. 2018). We extracted 545 high-quality spectra and HI widths for galaxies which passed the 2MTF selection criteria from the complete ALFALFA catalog. For consistency with the GBT and Parkes analysis, we used the W_{F50} width measurements.

2.2.3 Archival data

Besides our own observations and the ALFALFA data, we also used HI widths from archival sources where the data was high quality. The largest archival data source we adopted was the Cornell HI digital archive (Springob et al. 2005) of HI observations of 9,000 galaxies ($cz < 28,000$ km s^{-1}), obtained from single-dish telescopes. According to the HI line quality, Springob et al. (2005)

marked the HI lines with codes G (Good), F (Fair), S (Single peak) and P (Poor). Only G (Good) and F (Fair) galaxies were accepted into the 2MTF catalog. A total of 711 HI widths from the Cornell HI digital archive were included.

HI width measurements from other sources were also included (Theureau et al. 1998, 2005, 2007; Mathewson, Ford & Buchhorn 1992; Paturel et al. 2003). We collected raw HI widths from these catalogs and corrected for observational effects following the same procedure as for our own observations (for more details, see Hong et al. 2013).

2.2.4 Data Selection

To improve the distance measurement accuracy, further data quality limits were adopted. Galaxies with $cz < 600$ km s^{-1} (CMB frame), HI spectra with S/N ratio < 5, or relative HI error $\epsilon_{\rm w}/w_{\rm HI} > 10\%$ were omitted. When one galaxy was observed with more than one telescope, we preferred the newer data, i.e., our own observations and ALFALFA data have higher priority than the archival data.

2MASX J00383973+1724113 has a reported 2MASS axis ratio of b/a = 0.36, which doesn't represent the outer blue disk present in the galaxy. We give this galaxy a flag of 'W' in final data table, for optional exclusion.

2.3 Tully-Fisher distances

For calculating the Tully-Fisher distances and peculiar velocities for 2MTF galaxies, we use the TF template relations developed by Masters, Springob & Huchra (2008):

$$\begin{aligned} M_K - 5\log h &= -22.188 - 10.74(\log W - 2.5), \\ M_H - 5\log h &= -21.951 - 10.65(\log W - 2.5), \\ M_J - 5\log h &= -21.370 - 10.61(\log W - 2.5), \end{aligned} \quad (2)$$

where M_K, M_H, and M_J are the absolute magnitudes and W is the corrected HI linewidth. The TF template relation depends on the galaxy morphology in all bands; the above relations refer to galaxies of type Sc.

As described in Hong et al. (2014), the uncertainties of TF peculiar velocities are log-normal. So the preferred way to quote distances for 2MTF is the logarithmic quantity $\log(d_z/d_{\rm TF})$,

$$\log\left(\frac{d_z}{d^*_{\rm TF}}\right) = \frac{-\Delta M}{5}, \quad (3)$$

where d_z is the redshift distance of the galaxy in the CMB frame, $d^*_{\rm TF}$ is the galaxy's redshift-independent distance from the TF relation before Malmquist bias correction (which will be corrected in the final step of the calculation), and $\Delta M = M_{obs} - M(W)$ is the difference between the absolute magnitude calculated using a redshift distance and the absolute magnitude predicted by the TF template relations of Equation 2. The corrected absolute magnitude M_{obs} contains the terms for K-correction (k_X), extinction correction due to the Galaxy (A_X), internal extinction correction of the galaxy itself (I_X) and the morphological type correction T_X which arises from the different slopes and zero points of the TF relation between different types of galaxies, we adopt the same equation as Masters, Springob & Huchra (2008) of

$$M_{obs} - 5\log h = m_{obs} + k_X - A_X - I_X - T_X - 5\log v_{CMB} - 15, \quad (4)$$

where X represents K, H or J, v_{CMB} is the recession velocity of the galaxy in the CMB frame. We make all corrections following Masters, Springob & Huchra (2008).

The error in this logarithmic quantity includes four components: intrinsic error, inclination error, HI width error and NIR magnitude error (see Section 3.2 and Appendix A of Hong et al. 2014, for more details), where we adopt an intrinsic error inversely proportional to the HI width to represent the fact that the scatter of the TF relation decreases with the HI width (Giovanelli et al. 1997; Masters et al. 2006). The error in redshift is considered negligible because of its much higher accuracy. The final error in the logarithmic quantity is the sum in quadrature of all components in logarithmic units. To improve measurement accuracy, we used the galaxy group information presented by Crook et al. (2007) to assign the same redshift distance d_z to all galaxies in the same group, whilst $\log(d_z/d_{\rm TF})$ was calculated separately.

The final step of data reduction is the Malmquist bias correction. There are two types of Malmquist bias. Homogeneous Malmquist bias which arises from distance-dependent selection effects. This bias affects all galaxies regardless of their position. Inhomogeneous Malmquist bias is caused by the variation of density along the line of sight. As described by Strauss & Willick (1995), this bias is smaller in redshift space than distance space because of much smaller measurement errors. Thus we corrected for homogeneous Malmquist bias only, and considered the inhomogeneous bias to be negligible. We divided the sample into two parts north and south of declination $\delta = -40^\circ$, which reflects the fact that the completeness is different in these two sky regions. Corrections were made using the procedure of Hong et al. (2014), which in turn follows the procedure of Springob et al. (2014).

3 CATALOG PRESENTATION

We present the photometric data from 2MRS catalog and corrected HI widths for the 2,062 2MTF galaxies in Table 1. The definition of the columns of the table is as follows:

Column (1). — The 2MASS XSC ID name.

Column (2) and (3). — Right ascension (RA) and declination (DEC) in the J2000.0 epoch from the 2MASS XSC.

Column (4). — The barycentric redshift $cz_{\rm 2MRS}$ from the 2MRS (km s^{-1}).

Column (5 - 7). — The NIR magnitudes in the K, H and J bands from the 2MASS XSC, respectively.

Column (8 - 10). — The errors of the NIR magnitudes in K, H and J bands from the 2MASS XSC.

Column (11). — The corrected HI width (km s^{-1}).

Column (12). — The error of corrected HI width (km s^{-1}).

Table 2 contains the logarithmic distance quantity measured by 2MTF, together with linear peculiar velocities defined by Eq. (1), the latter is provided for convenience. We also include the peculiar velocities generated from the estimator introduced by Watkins & Feldman (2015):

$$V_{WF15} = cz\ln(cz/H_0 r) = cz\ln(d_z/d_{\rm TF}), \quad (5)$$

where z is the redshift of the galaxy and r is the redshift-independent distance (the Tully-Fisher distance in this paper). We adopt a low redshift approximation of the accurate WF15 estimator (Eq. 7 of Watkins & Feldman 2015) here, since the redshift of 2MTF galaxies is much smaller than unity. All measurements are made in the CMB reference frame, so we convert

Table 1. Photometric and corrected HI width data for 2MTF galaxies.

2MASX-ID	RA [deg] (J2000)	DEC [deg] (J2000)	cz_{2MRS} [km s^{-1}]	m_K [mag]	m_H [mag]	m_J [mag]	ϵ_{m_K} [mag]	ϵ_{m_H} [mag]	ϵ_{m_J} [mag]	W_c [km s^{-1}]	ϵ_{W_c} [km s^{-1}]
00005604+2020165	0.23345	20.33799	6804	11.124	11.616	12.339	0.061	0.062	0.046	406	5.1
00005891+2854421	0.24550	28.91172	6899	10.818	11.085	11.515	0.059	0.048	0.029	440	11.8
00010478+0432261	0.26987	4.54060	9151	11.029	11.274	11.919	0.047	0.036	0.026	476	23.0
00011976+3431326	0.33238	34.52571	5032	10.405	10.704	11.384	0.037	0.028	0.023	439	5.9
00013830+2329011	0.40968	23.48363	4371	9.330	9.591	10.327	0.024	0.021	0.019	544	8.0
00014193+2329452	0.42471	23.49588	4336	9.930	10.154	11.056	0.025	0.021	0.019	635	10.6
00024636+1853106	0.69321	18.88622	7882	10.776	10.935	11.652	0.042	0.032	0.027	518	11.2
00035889+2045084	0.99545	20.75235	2309	8.400	8.700	9.438	0.008	0.007	0.006	384	6.0
00041299+1047258	1.05410	10.79052	7887	10.678	10.943	11.652	0.045	0.036	0.029	412	12.2
00051672-1628368	1.31967	−16.47691	7412	10.135	10.448	11.174	0.028	0.026	0.020	528	12.1
00055236+2232083	1.46812	22.53567	6644	11.221	11.520	12.320	0.045	0.039	0.037	273	6.5
00064016+2609164	1.66731	26.15452	7556	10.965	11.338	11.938	0.045	0.044	0.034	393	14.7
00071951+3236334	1.83139	32.60925	5076	9.865	10.136	10.914	0.026	0.022	0.019	461	4.8
00080679+0943037	2.02831	9.71773	6423	10.523	10.826	11.450	0.049	0.041	0.033	408	9.2
00084772+3326000	2.19883	33.43332	4808	9.731	9.974	10.639	0.027	0.024	0.020	457	5.5
00090421+1055081	2.26760	10.91890	6674	10.605	10.974	11.870	0.043	0.035	0.033	464	4.6
00092866+4721208	2.36937	47.35583	5153	11.218	11.562	12.181	0.066	0.062	0.045	308	11.8
00093281+4808068	2.38672	48.13519	5388	11.018	11.229	11.965	0.046	0.039	0.032	384	11.2
00102637+2859164	2.60990	28.98794	7850	11.171	11.552	12.460	0.046	0.041	0.039	432	8.2
00103277+2859464	2.63654	28.99624	7033	10.409	10.648	11.435	0.033	0.024	0.024	428	24.3
00111259-3334428	2.80248	−33.57855	7853	10.295	10.601	11.187	0.044	0.034	0.021	503	41.9
00121573+2219187	3.06553	22.32180	7629	10.584	10.896	11.571	0.034	0.024	0.023	514	9.3
00143187-0044156	3.63279	−0.73760	3946	11.028	11.312	11.984	0.069	0.056	0.046	310	7.1
00144010+1834551	3.66711	18.58203	5392	9.479	9.843	10.654	0.024	0.016	0.015	554	5.5
00155127+1605232	3.96365	16.08977	4213	10.509	10.813	11.550	0.040	0.028	0.022	298	6.6
00164417+0704337	4.18407	7.07609	3966	9.750	10.099	10.873	0.022	0.016	0.016	387	4.8
00165087-0516060	4.21202	−5.26830	3968	10.510	10.800	11.449	0.055	0.044	0.033	268	21.0
00180131-5905008	4.50560	−59.08359	8924	11.072	11.464	12.346	0.053	0.041	0.039	443	22.5
00181053+1817323	4.54393	18.29227	5521	11.219	11.439	12.253	0.058	0.031	0.034	349	5.1
00183335-0616195	4.63899	−6.27206	6520	11.116	11.436	12.205	0.044	0.037	0.033	277	12.0

Table 1 is available in its entirety online. A portion is shown here for guidance regarding its form and content.

the recession velocities of galaxies to this frame using a solar motion of $v = 384$ km s^{-1} towards to $(l, b) = (263.99°, 48.26°)$ (Planck Collaboration et al. 2014b). Table 2 is organized as follows:

Column (1). — The 2MASS XSC ID name.

Column (2). — The CMB frame redshift $cz_{\rm CMB}$ (km s^{-1}).

Column (3 - 5). — The logarithmic quantities and errors measured by K, H and J band magnitude, respectively.

Column (6 - 8). — The peculiar velocities and errors measured by K, H and J band magnitude, respectively (km s^{-1}).

Column (9 - 11). — The peculiar velocities and errors calculated by WF15 estimator in K, H and J band magnitude, respectively (km s^{-1}).

Column (12). — Data quality warning flag, a flag 'W' reminds one to use the measurement of the galaxy carefully.

Fig. 1 and Fig. 2 show the sky coverage and redshift distribution, respectively, of the final 2MTF catalogue which contains 2,062 galaxies with good data quality. As shown in Fig. 1, the 2MTF catalog provides a fairly uniform distribution across the sky with a narrow gap near the Galactic plane ($|b| \leqslant 5°$). In the southern sky $\delta < -40°$, the target density is lower because we have only Parkes observations in this area. Galaxies in the final 2MTF catalogue cover a CMB velocity range of 600 km s^{-1} $< cz < 10,000$ km s^{-1} with a mean velocity of $cz = 4,805$ km s^{-1}.

Fig. 3 shows the relative errors of the linear TF distances measured in the three 2MASS bands. The mean relative errors are 22%, 22% and 23% in the K, H and J bands respectively.

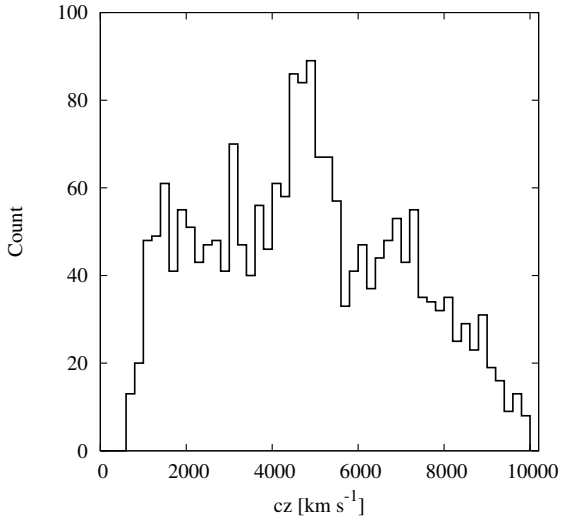

Figure 2. The redshift distribution of 2,062 2MTF galaxies in the CMB frame.

4 COMPARISON WITH COSMICFLOWS-3

We compare the 2MTF redshift-independent distances with the distances listed in the Cosmicflows-3 catalogue (Tully, Courtois & Sorce 2016). The Cosmicflows-3 catalogue includes around 17,700 distances, measured by various authors and various methods, mainly Tully-Fisher and Fundamental Plane.

Table 2 Distances and peculiar velocities for 2,062 2MTF galaxies.

2MASX ID	cz_{CMB}	$\log \frac{d_z}{d_{\rm TF,K}}$	$\log \frac{d_z}{d_{\rm TF,H}}$	$\log \frac{d_z}{d_{\rm TF,J}}$	$V_{pec,K}$	$V_{pec,H}$	$V_{pec,J}$	$V_{WF15,K}$	$V_{WF15,H}$	$V_{WF15,J}$	Flag
- -	[km s^{-1}]	[- -]	[- -]	[- -]	[km s^{-1}]						[- -]
(1)	(2)	(3)	(4)	(5)	(6)	(7)	(8)	(9)	(10)	(11)	(12)
00005604+2020165	6439	-0.127 ± 0.078	-0.156 ± 0.075	-0.160 ± 0.080	-2165 ± 389	-2756 ± 476	-2843 ± 524	-1889 ± 1152	-2316 ± 1110	-2377 ± 1185	–
00005891+2854421	6546	-0.071 ± 0.092	-0.057 ± 0.088	-0.023 ± 0.093	-1145 ± 243	-907 ± 184	-340 ± 73	-1066 ± 1388	-859 ± 1334	-342 ± 1406	–
00010478+0432261	8717	-0.061 ± 0.091	-0.042 ± 0.087	-0.041 ± 0.092	-1265 ± 265	-838 ± 170	-823 ± 174	-1226 ± 1827	-845 ± 1756	-831 ± 1851	–
00011976+3431326	4694	-0.092 ± 0.083	-0.081 ± 0.079	-0.081 ± 0.085	-1106 ± 211	-964 ± 175	-956 ± 187	-995 ± 896	-879 ± 857	-873 ± 922	–
00013830+2329011	3982	-0.218 ± 0.075	-0.200 ± 0.070	-0.212 ± 0.077	-2582 ± 452	-2318 ± 374	-2491 ± 442	-1996 ± 692	-1833 ± 641	-1941 ± 705	–
00014193+2329452	4018	-0.385 ± 0.069	-0.352 ± 0.062	-0.382 ± 0.069	-5768 ± 916	-5053 ± 721	-5717 ± 908	-3559 ± 636	-3254 ± 575	-3538 ± 638	–
00024636+1853106	7516	-0.069 ± 0.084	-0.027 ± 0.078	-0.035 ± 0.084	-1252 ± 242	-451 ± 81	-605 ± 117	-1187 ± 1449	-467 ± 1352	-611 ± 1454	–
00035889+2045084	1946	0.027 ± 0.087	0.038 ± 0.085	0.035 ± 0.091	120 ± 24	164 ± 32	152 ± 32	123 ± 391	170 ± 380	158 ± 407	–
00041299+1047258	7601	0.073 ± 0.097	0.083 ± 0.093	0.078 ± 0.098	1192 ± 266	1341 ± 287	1271 ± 287	1271 ± 1696	1449 ± 1633	1365 ± 1720	–
00051672-1628368	7086	-0.111 ± 0.076	-0.102 ± 0.070	-0.116 ± 0.077	-2037 ± 357	-1864 ± 305	-2149 ± 381	-1806 ± 1243	-1671 ± 1150	-1893 ± 1263	–
00055236+2232083	6237	0.208 ± 0.117	0.203 ± 0.118	0.181 ± 0.120	2369 ± 638	2330 ± 633	2128 ± 588	2983 ± 1675	2920 ± 1696	2605 ± 1728	–
00064016+2609164	7203	0.023 ± 0.092	0.016 ± 0.090	0.030 ± 0.095	389 ± 83	274 ± 57	488 ± 107	386 ± 1534	265 ± 1489	491 ± 1571	–
00071951+3236334	4608	-0.083 ± 0.076	-0.064 ± 0.072	-0.076 ± 0.079	-1041 ± 182	-792 ± 131	-942 ± 171	-885 ± 810	-677 ± 760	-804 ± 835	–
00080679+0943037	6043	0.057 ± 0.100	0.057 ± 0.098	0.063 ± 0.102	749 ± 172	749 ± 169	824 ± 193	786 ± 1384	788 ± 1362	872 ± 1418	–
00084772+3326000	4608	-0.052 ± 0.077	-0.029 ± 0.074	-0.026 ± 0.080	-648 ± 115	-369 ± 63	-340 ± 63	-554 ± 821	-302 ± 782	-275 ± 847	–
00090421+1055081	6310	-0.057 ± 0.077	-0.058 ± 0.072	-0.082 ± 0.079	-871 ± 154	-891 ± 148	-1297 ± 236	-828 ± 1122	-846 ± 1053	-1191 ± 1142	–
00092866+4721208	4884	0.003 ± 0.107	-0.004 ± 0.108	0.002 ± 0.111	50 ± 12	-35 ± 9	40 ± 10	36 ± 1206	-48 ± 1211	27 ± 1245	–
00093281+4808068	4976	-0.163 ± 0.103	-0.137 ± 0.100	-0.155 ± 0.105	-2241 ± 532	-1828 ± 421	-2111 ± 510	-1866 ± 1179	-1573 ± 1149	-1776 ± 1205	–
00102637+2859164	7507	-0.097 ± 0.076	-0.099 ± 0.073	-0.133 ± 0.079	-1843 ± 322	-1893 ± 318	-2662 ± 484	-1668 ± 1322	-1710 ± 1257	-2299 ± 1362	–
00103277+2859464	6677	-0.014 ± 0.103	0.003 ± 0.100	-0.018 ± 0.104	-199 ± 47	63 ± 14	-267 ± 64	-218 ± 1579	42 ± 1539	-284 ± 1600	–
00111259-3334428	7586	-0.042 ± 0.107	-0.038 ± 0.104	-0.019 ± 0.107	-763 ± 188	-683 ± 164	-329 ± 81	-737 ± 1873	-666 ± 1811	-334 ± 1876	–
00121573+2219187	7258	-0.063 ± 0.078	-0.055 ± 0.072	-0.056 ± 0.079	-1121 ± 201	-962 ± 159	-993 ± 181	-1051 ± 1302	-912 ± 1207	-939 ± 1322	–
00143187-0044156	3589	-0.097 ± 0.109	-0.101 ± 0.109	-0.106 ± 0.112	-893 ± 224	-935 ± 235	-987 ± 254	-798 ± 897	-832 ± 902	-873 ± 926	–
00144010+1834551	5037	-0.056 ± 0.065	-0.051 ± 0.057	-0.058 ± 0.066	-703 ± 105	-638 ± 84	-726 ± 110	-646 ± 753	-589 ± 662	-667 ± 768	–
00155127+1605232	3838	0.108 ± 0.101	0.112 ± 0.102	0.106 ± 0.105	830 ± 193	857 ± 201	816 ± 197	954 ± 895	989 ± 901	936 ± 927	–
00164417+0704337	3598	0.019 ± 0.084	0.021 ± 0.082	0.016 ± 0.087	133 ± 26	154 ± 29	108 ± 22	155 ± 698	177 ± 678	130 ± 719	–
00165087-0516060	3597	0.159 ± 0.132	0.159 ± 0.134	0.161 ± 0.135	1088 ± 328	1088 ± 336	1099 ± 342	1316 ± 1089	1315 ± 1112	1332 ± 1120	–
00180131-5905008	8707	-0.011 ± 0.090	-0.021 ± 0.086	-0.050 ± 0.091	-185 ± 38	-401 ± 79	-1022 ± 214	-219 ± 1804	-427 ± 1730	-1002 ± 1828	–
00181053+1817323	5150	-0.094 ± 0.089	-0.063 ± 0.088	-0.080 ± 0.092	-1224 ± 251	-790 ± 160	-1020 ± 218	-1110 ± 1057	-747 ± 1049	-943 ± 1097	–
00183335-0616195	6064	0.119 ± 0.121	0.116 ± 0.122	0.099 ± 0.124	1457 ± 406	1427 ± 401	1235 ± 353	1663 ± 1684	1624 ± 1705	1378 ± 1736	–

Table 2 is available in its entirety online. A portion is shown here for guidance regarding form and content.

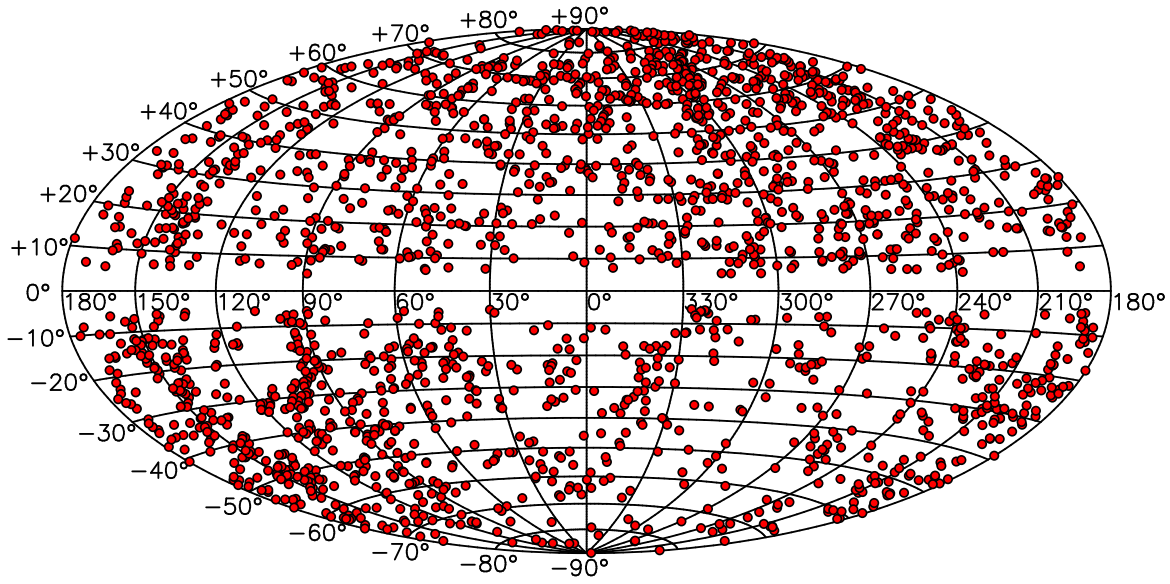

Figure 1. Sky coverage of the 2,062 2MTF galaxies, in Galactic coordinates using an Aitoff projection.

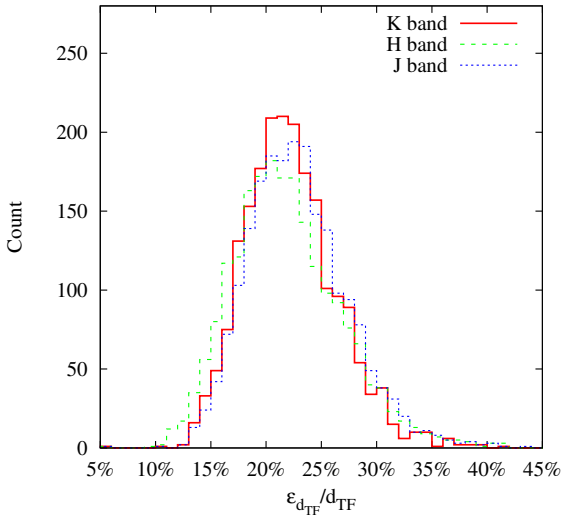

Figure 3. Relative errors of the TF distances measured in the K (red solid line), H (green dashed line) and J (blue dotted line) bands.

Cross-matching 2MTF with Cosmicflows-3 by sky position and redshift, we found 1,117 common galaxies within a velocity difference $|cz| \leqslant 150$ km s^{-1}. A comparison of the distance moduli of the 2MTF and Cosmicflows-3 measurements reveals only a few outliers far from the line of distance equality. On the whole, there is excellent agreement as shown in Fig. 4. With a 3σ outlier clip, the mean difference between Cosmicflows-3 and 2MTF measurements are 0.03 ± 0.01 mag, 0.06 ± 0.01 mag and 0.06 ± 0.01 mag in the K, H and J bands respectively. The corresponding scatter is 0.35, 0.34 and 0.33 mag, respectively. For linear distances, We find the Cosmicflows-3 measurements are 1.4%, 2.8% and 2.8% larger than 2MTF distances in three bands respectively. These results are consistent with those reported by Qin et al. (2019).

Cosmicflows-3 also contains a compilation of 391 supernova type Ia (SNIa) distances for redshifts $z \leqslant 0.1$, with the distance modulus provided being the average of multiple measurements, where available. Modern SNIa distances can be highly accurate (e.g. Jha, Riess & Kirshner 2007; Amanullah et al. 2010), and thus allow a more stringent test of 2MTF data quality. A cross-match between 2MTF and Cosmicflows-3 SNIa distances finds 28 galaxies which have hosted SNIa events. We present the comparison of the distance moduli in Fig. 5. Again, no significant systematic bias in 2MTF distance measurements is found, with the mean difference between 2MTF and Cosmicflows-3 measurements being 0.12 ± 0.08 mag with a standard deviation of 0.40 mag. However, the outlier in this plot is 2MASS 09220265+5058353 which hosted SN 1999b. According to the NASA/IPAC Extragalactic Database (NED), the distance moduli measured using SN 1999b vary from 30.20 to 31.16 mag, compared with our larger K-band 2MTF measurement of 32.22 ± 0.43 mag. Neglecting this outlier, the mean difference between 2MTF and Cosmicflows-3 SNIa measurements is only 0.08 ± 0.06 mag with a standard deviation of 0.32 mag. In linear distance space, we find the Cosmicflows-3 SNIa measurements are 3.7% smaller than 2MTF distances in mean, the opposite trend of the whole Cosmicflows-3 sample. However, the difference is not significant.

5 BULK FLOW IN THE FULL 2MTF SAMPLE

Bulk flow is measured from the dipole of the peculiar velocity field, and represents the averaged peculiar motion of the galaxies in the survey volume with respect to the CMB. In standard theory, it is believed to arise from acceleration induced by mass distributions within and beyond the sample volume, and therefore provides a useful probe of the mass distribution in the local Universe. It is also a powerful tool to test different cosmological models (e.g. Hudson et al. 2004; Ma & Scott 2013; Ma & Pan 2014; Hong et al. 2014; Scrimgeour et al. 2016; Qin et al. 2018, and references therein). The high-accuracy distance estimates, the well-defined selection function, and the uniform sky coverage of 2MTF makes this survey easier to use for bulk flow measurements.

Using the preliminary 2MTF sample, Hong et al. (2014) measured the bulk flow at the depths of 20 h^{-1}Mpc, 30 h^{-1}Mpc and 40 h^{-1}Mpc, and found the amplitude to be within the range of the ΛCDM model. Qin et al. (2018) combined the 2MTF catalog with the 6dFGSv survey, making an accurate bulk flow measurement at

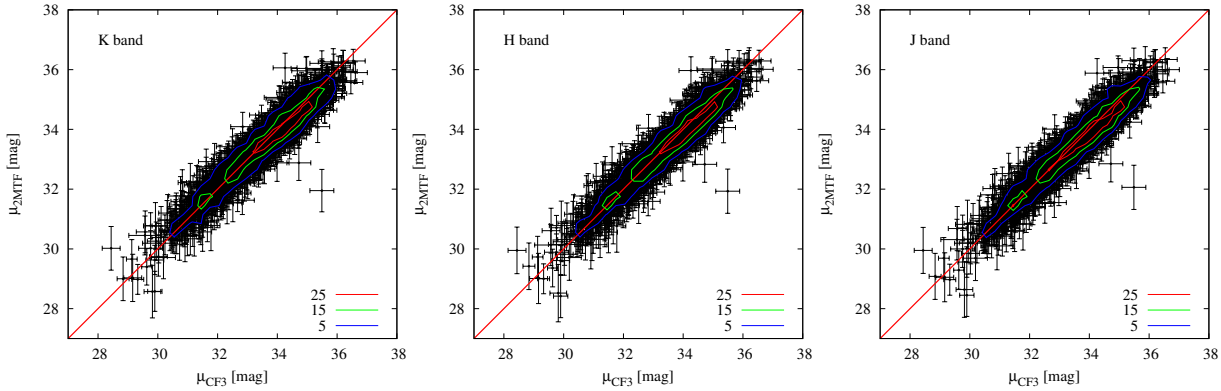

Figure 4. Comparison of the distance moduli for 1,117 galaxies common between Cosmicflows-3 and 2MTF in the K, H and J bands, respectively. The red solid line indicates equality. The galaxy number density in 0.5 mag $\times$ 0.5 mag cells is represented by the colour contours. The outlier far away from the equality line at the bottom right is the galaxy 2MASX J00383973+1724113 for which we give the flag 'W' in Table 2.

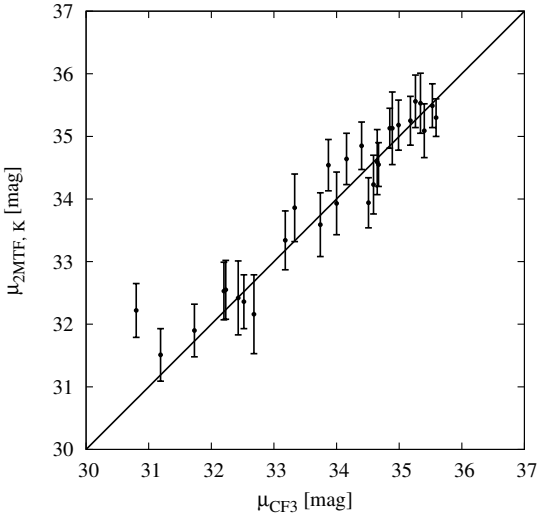

Figure 5. Comparison of 28 distances moduli for galaxies measured in 2MTF (K band) which host SNIa catalogued in Cosmicflows-3. The solid line indicates equality.

the scale of 40 h^{-1}Mpc, and again showed consistency with the ΛCDM model.

In this paper, we measured the bulk flow of the final 2MTF sample using the χ^2 minimization method of Hong et al. (2014):

$$\chi^2 = \sum_{i=1}^{N} \frac{[\log(d_{z,i}/d_{\mathrm{model},i}) - \log(d_{z,i}/d_{\mathrm{TF},i})]^2 \cdot w_i^r w_i^d}{\sigma_i^2 \cdot \sum_{i=1}^{N}(w_i^r w_i^d)}, \quad (6)$$

where $d_{\mathrm{model},i}$ is the model-predicted distance of the i'th galaxy, σ_i is the error of i'th galaxy's logarithmic distance ratio $\log(d_z/d_{TF})$, w_i^r is the weight to make the sample's weighted redshift distribution match a Gaussian function at a number of depths (here we choose R_I = 20, 30 and 40 h^{-1}Mpc), w_i^d is the weight to correct for the effect of the slightly different number density in the northern and southern sky areas (see Section 4.1 of Hong et al. 2014, for more details). Instead of using the peculiar velocity data from individual bands, we combine the data from all K, H and J bands into a '3-bands combined sample' for greatest accuracy. In the combined sample, every galaxy is used three times with different peculiar velocities measured from three different bands, with each peculiar velocity counted separately during the minimization procedure. As the errors in our TF distances are log-normal, this fit process works in log space instead of linear space. The fitting method is less sophisticated than the ηMLE technique of Qin et al. (2018) which can, in principle, model generic non-normal error distributions. But, since the major errors in 2MTF are the multiplicative distance errors, the current technique is more than adequate. Moreover, it allows a more straightforward comparison with our previous results. The errors of the bulk flow velocities were estimated using the jackknife method with 50 sub-samples, randomly selected by removing 2% of the 2MTF sample each time.

Table 3. Bulk flow amplitudes measured in the 2MTF sample.

	Hong et al. (2014) [km s^{-1}]	this work [km s^{-1}]
$R_I = 20\ h^{-1}$Mpc	310.9 ± 33.9	307.8 ± 25.9
$R_I = 30\ h^{-1}$Mpc	280.8 ± 25.0	317.6 ± 29.4
$R_I = 40\ h^{-1}$Mpc	292.3 ± 27.8	286.1 ± 25.5

The theoretical prediction of the bulk flow amplitude varies with the depth of the galaxy sample (Ma & Pan 2014), so our theoretical curve was calculated using a Gaussian window function $W(kR) = \exp(-k^2R^2)/2$ and a matter power spectrum $P(k)$ generated by the CAMB package (Lewis, Challinor & Lasenby 2000):

$$v_{\mathrm{rms}}^2 = \frac{H_0^2 f^2}{2\pi^2} \int W^2(kR) P(k) \mathrm{d}k, \quad (7)$$

where k is the wavenumber, H_0 is the Hubble constant and $f = \Omega_{\mathrm{m}}^{0.55}$ is the linear growth rate (Li et al. 2012; Hong et al. 2014). For the calculation of the theoretical curves, we adopt the cosmological parameters reported by Planck Collaboration et al. (2016) with $\Omega_m = 0.308$, $\Omega_b = 0.0484$, $n_s = 0.9677$ and $\mathrm{H}_0 = 67.81$ km s^{-1} Mpc^{-1}.

The best-fit bulk flow velocities for the three different depths are presented in the Table 3 together with the results measured by Hong et al. (2014) using the preliminary 2MTF sample. We also plot the bulk flow velocity amplitudes in Fig. 6, where the solid line is the ΛCDM prediction and the dashed lines indicate the $\pm 1\sigma$ points of the theoretical line (i.e. ± 34 per cent). The best-fit bulk flows agree with our previous measurements but have smaller uncertainties, mainly because the new sample has a larger size and the updated ALFALFA data has higher accuracy than the previous archival data. Again, our results are consistent with the ΛCDM model prediction at 68% confidence level, which supports the correctness of the ΛCDM model in the local Universe.

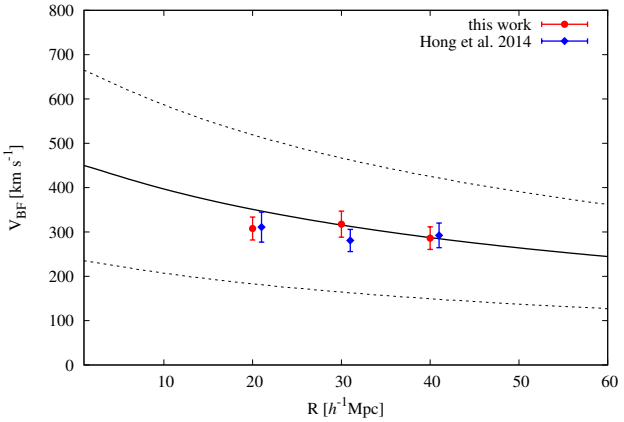

Figure 6. The bulk flow amplitude measured using the three-band combined sample at the scale of 20, 30 and 40 $h^{-1}\mathrm{Mpc}$, respectively (red dots). The results of Hong et al. (2014) using the preliminary 2MTF sample are plotted using the blue diamonds (shifted 1 $h^{-1}\mathrm{Mpc}$ right for clarity). The solid line shows the ΛCDM theoretical prediction, and the dashed lines are the 68% confidence level of the sample expectation.

6 SUMMARY

2MTF is an all-sky survey which provides accurate Tully-Fisher distances for galaxies in the local Universe with a well-defined selection function. Due to the use of near-infrared photometry, the survey has more uniform sky coverage than similar previous surveys. The Zone of Avoidance around the Galactic plane is only $|b| \leqslant 5°$.

Together with good quality HI data from new observations, the ALFALFA survey and high signal-to-noise ratio archival data, 2MTF provides high-accuracy distance measurements for 2,062 nearby spiral galaxies. The mean relative error in the final 2MTF sample is 22%. We compare our measurements with the published distances in Cosmicflows-3, which represents the largest compendium of nearby galaxy distances. We find no substantial systematic difference between 2MTF and Cosmicflows-3 distances. Higher accuracy SNe Ia distances were also compared for 28 cross-matched objects. Again, no substantial systematic difference was found.

The best-fit bulk flow velocity amplitudes are $V = 308 \pm 26$ km s^{-1}, $V = 318 \pm 29$ km s^{-1}, and $V = 286 \pm 25$ km s^{-1}at depths of $R_I = 20$, 30 and 40 $h^{-1}\mathrm{Mpc}$ respectively, consistent with our previous measurements using the preliminary 2MTF sample but with higher accuracy. The fit results agree with the ΛCDM prediction at the 68% confidence level.

ACKNOWLEDGMENTS

The authors wish to acknowledge the contributions of John Huchra (1948 - 2010) to this work. The 2MTF survey was initiated while KLM was a post-doc working with John at Harvard, and its design owes much to his advice and insight. This work was partially supported by NSF grant AST- 0406906 to PI John Huchra.

Parts of this research were conducted by the Australian Research Council Centre of Excellence for All-sky Astrophysics (CAASTRO), through project number CE110001020, and the Australian Research Council Centre of Excellence for All Sky Astrophysics in 3 Dimensions (ASTRO 3D), through project number CE170100013. TH was supported by the National Natural Science Foundation of China (Grant No. 11473034, U1731127), the Key Research Program of the Chinese Academy of Sciences (Grant No. QYZDJ-SSW-SLH021), the strategic Priority Research Program of Chinese Academy of Sciences (Grant No. XDB23010200), and the Open Project Program of the Key Laboratory of FAST, NAOC, Chinese Academy of Sciences.

REFERENCES

Alpaslan M. et al., 2014, MNRAS, 438, 177
Amanullah R. et al., 2010, ApJ, 716, 712
Andersen P., Davis T. M., Howlett C., 2016, MNRAS, 463, 4083
Bautista J. E. et al., 2017, ArXiv e-prints
Bernardeau F., Colombi S., Gaztañaga E., Scoccimarro R., 2002, Phys. Rep., 367, 1
Brunthaler A., Reid M. J., Falcke H., Greenhill L. J., Henkel C., 2005, Science, 307, 1440
Campbell L. A. et al., 2014, MNRAS, 443, 1231
Crook A. C., Huchra J. P., Martimbeau N., Masters K. L., Jarrett T., Macri L. M., 2007, ApJ, 655, 790
Dressler A., Lynden-Bell D., Burstein D., Davies R. L., Faber S. M., Terlevich R., Wegner G., 1987, ApJ, 313, 42
Eisenstein D. J. et al., 2005, ApJ, 633, 560
Geller M. J., Huchra J. P., 1989, Science, 246, 897
Giovanelli R., Haynes M. P., Herter T., Vogt N. P., da Costa L. N., Freudling, W.and Salzer J. J., Wegner G., 1997, AJ, 113, 53
Giovanelli R. et al., 2005, AJ, 130, 2598
Gott, III J. R., Jurić M., Schlegel D., Hoyle F., Vogeley M., Tegmark M., Bahcall N., Brinkmann J., 2005, ApJ, 624, 463
Haynes M. P. et al., 2018, ArXiv e-prints
Hong T., Han J. L., Wen Z. L., 2016, ApJ, 826, 154
Hong T. et al., 2014, MNRAS, 445, 402
Hong T. et al., 2013, MNRAS, 432, 1178
Huchra J. P. et al., 2012, ApJS, 199, 26
Hudson M. J., Smith R. J., Lucey J. R., Branchini E., 2004, MNRAS, 352, 61
Jha S., Riess A. G., Kirshner R. P., 2007, ApJ, 659, 122
Jones D. H. et al., 2009, MNRAS, 399, 683
Kashlinsky A., Atrio-Barandela F., Ebeling H., 2011, ApJ, 732, 1
Kraan-Korteweg R. C., Cluver M. E., Bilicki M., Jarrett T. H., Colless M., Elagali A., Böhringer H., Chon G., 2017, MNRAS, 466, L29
Kraan-Korteweg R. C., Lahav O., 2000, A&A Rev., 10, 211
Lewis A., Challinor A., Lasenby A., 2000, ApJ, 538, 473
Li M. et al., 2012, ApJ, 761, 151
Lombriser L., Slosar A., Seljak U., Hu W., 2012, Phys. Rev. D, 85, 124038
Ma Y.-Z., Pan J., 2014, MNRAS, 437, 1996
Ma Y.-Z., Scott D., 2013, MNRAS, 428, 2017
Masters K. L., Crook A., Hong T., Jarrett T. H., Koribalski B. S., Macri L., Springob C. M., Staveley-Smith L., 2014, MNRAS, 443, 1044
Masters K. L., Springob C. M., Haynes M. P., Giovanelli R., 2006, ApJ, 653, 861
Masters K. L., Springob C. M., Huchra J. P., 2008, AJ, 135, 1738
Mathewson D. S., Ford V. L., Buchhorn M., 1992, ApJS, 81, 413
Paturel G., Theureau G., Bottinelli L., Gouguenheim L., Coudreau-Durand N., Hallet N., Petit C., 2003, A&A, 412, 57
Phillips M. M., 1993, ApJ, 413, L105
Planck Collaboration et al., 2014a, A&A, 571, A17
Planck Collaboration et al., 2016, A&A, 594, A13

Planck Collaboration et al., 2014b, A&A, 571, A27
Qin F., Howlett C., Staveley-Smith L., Hong T., 2018, MNRAS, 477, 5150
Qin F., Howlett C., Staveley-Smith L., Hong T., 2019, MNRAS, 482, 1920
Salvati L., Douspis M., Aghanim N., 2018, A&A, 614, A13
Scrimgeour M. I. et al., 2012, MNRAS, 425, 116
Scrimgeour M. I. et al., 2016, MNRAS, 455, 386
Springob C. M., Haynes M. P., Giovanelli R., Kent B. R., 2005, ApJS, 160, 149
Springob C. M. et al., 2016, MNRAS, 456, 1886
Springob C. M. et al., 2014, MNRAS, 445, 2677
Springob C. M., Masters K. L., Haynes M. P., Giovanelli R., Marinoni C., 2007, ApJS, 172, 599
Strauss M. A., Willick J. A., 1995, Phys. Rep., 261, 271
Theureau G., Bottinelli L., Coudreau-Durand N., Gouguenheim L., Hallet N., Loulergue M., Paturel G., Teerikorpi P., 1998, A&AS, 130, 333
Theureau G. et al., 2005, A&A, 430, 373
Theureau G., Hanski M. O., Coudreau N., Hallet N., Martin J.-M., 2007, A&A, 465, 71
Tonry J., Schneider D. P., 1988, AJ, 96, 807
Tully R. B., Courtois H. M., Sorce J. G., 2016, AJ, 152, 50
Tully R. B., Fisher J. R., 1977, A&A, 54, 661
Van Waerbeke L. et al., 2013, MNRAS, 433, 3373
Watkins R., Feldman H. A., 2015, MNRAS, 450, 1868